Precrystallization solute assemblies and crystal symmetry

Monika Warzecha,[1,‡] Lakshmanji Verma,[2,‡] Rajshree Chakrabarti,[2,‡] Viktor G. Hadjiev,[3] Alastair Florence,[1] Jeremy Palmer,[2] and Peter Vekilov[2,4,*]

[1]*EPSRC CMAC Future Manufacturing Research Hub, c/o Strathclyde Institute of Pharmacy and Biomedical Sciences, Technology and Innovation Centre, 99 George Street, Glasgow, G1 1RD, U.K.*

[2]*Department of Chemical and Biomolecular Engineering, University of Houston, 4726 Calhoun Rd., Houston, TX 77204-4004, USA.*

[3]*Texas Center for Superconductivity, University of Houston, 3369 Cullen Blvd., Suite 202, Houston, Texas 77004-50024, USA*

[4]*Department of Chemistry, University of Houston, 3585 Cullen Blvd., Houston, TX 77204-5003, USA*

Abstract

Solution crystallization is a part of the synthesis of materials ranging from geological and biological minerals to pharmaceuticals, fine chemicals, and advanced electronic components. Attempts to predict the structure, growth rates and properties of emerging crystals have been frustrated, in part, by the poor understanding of the correlations between the oligomeric state of the solute, the growth unit, and the crystal symmetry. To explore how a solute monomer or oligomer is selected as the unit that incorporates into kinks and how crystal symmetry impacts this selection we combine scanning probe microscopy, optical spectroscopy, and all-atom molecular simulations using as examples two organic materials, olanzapine (OZPN) and etioporphyrin I (EtpI). The dominance of dimeric structures in OZPN crystals has spurred speculation that the dimers preform in the solution, where they capture the majority of the solute, and then assemble into crystals. By contrast, EtpI in crystals aligns in parallel stacks of flat EtpI monomers unrelated by point symmetry. We show that solute monomers are the majority solution

species in solutions of both compounds. Surprisingly, the kinetics of incorporation of OZPN into kinks is bimolecular, indicating that the growth unit is a solute dimer, a minority solution component. The disconnection between the dominant solute species, the growth unit, and the crystal symmetry is even stronger with EtpI, for which the (010) face grows by incorporating monomers, whereas the growth unit of the (001) face is a dimer. Collectively, the crystallization kinetics results with OZPN and EtpI establish that the structures of the dominant solute species and of the incorporating solute complex do not correlate with the symmetry of the crystal lattice. In a broader context, these findings illuminate the immense complexity of crystallization scenarios that need to be explored on the road to understanding and control of crystallization.

Introduction

Crystals are defined by their symmetry.[1] Crystal symmetry combines point symmetry elements, such as an inversion centers, mirror planes, and rotation axes, typical of finite-size objects, with translation.[2] The translational symmetry of silicon, germanium, and other semiconductor crystals guides their electronic band structure and the behaviors of charge carriers that define their utility.[3] The point symmetry of diamond and other precious stones is lower than that of a sphere and governs their direction-dependent properties, including the substantial anisotropy of their refractive indexes, their most appealing property.[4] Alternatively, the lack of an inversion center in quartz and other polar crystals preconditions their piezoelectricity.[5] The hexagonal molecular arrangement in normal ice institutes a density lower than that of water and enforces ice accumulation on the surfaces of lakes and seas, which, in turn, facilitated the rise of life.[6]

Translational symmetry dictates exact rules for how a molecule in a crystal orients and positions with respect to any other crystal molecule. It arises during crystallization. The origin of point symmetry elements, however, is far less understood. Crystal point symmetry is certainly uncorrelated to molecular symmetry.[7, 8] Water molecules carry two-fold symmetry, yet at standard

conditions they crystalize as hexagonal ice. At elevated pressures and low temperatures water arranges in several other distinct crystal lattices. The variability of crystal symmetries that a single molecule can adopt, often called polymorphism, is another example of the disconnection between molecular and crystal symmetries.[9]

The classical theories of crystal nucleation and growth assume that molecules incorporate into a crystal individually. This perspective inevitably commands that, similarly to translational symmetry, point symmetry arises during crystallization. Recent observations in complex biological, geological, and synthetic environments have exposed cases of nonclassical crystallization employing liquid, amorphous, and crystalline precursors[10-15]. The agency of the mesoscopic precursors only marginally modifies our understanding of the correlation between solute and crystal symmetries since the ordered structures of nanocrystals originate during their own nucleation[11]; amorphous, liquid, or partially ordered[16, 17] particles attain symmetry upon conversion to crystals or association to a host crystal.

A more intriguing question is posed by microscopic crystallization precursors that present as solute dimers and higher order oligomers, which form owing to the unavoidable interactions between solute monomers[18-21] and may, in some cases, mirror the structural units of the crystal.[22-26] It is easy to presume that the common structural motifs in the solution and in the crystal represent the solute species that associate to the kinks, which would imply that crystal symmetry elements arise in the solution prior to crystallization. The elementary acts of incorporation into kinks, however, have only been directly visualized for relatively few crystals.[27-43] Given the constrains to directly identify the growth unit, the promotion of the solute oligomers to the rank of the incorporating species has remained largely unchallenged and the origin of crystal symmetry, obscure.

To test how solute oligomers transition into symmetry-related crystal blocks, here we put forth the kinetics of step growth as an indicator of the crystal growth unit. We then explore the

correlation of the growth unit with the state of the solute and the crystal symmetry. We use as examples of two molecular crystals, olanzapine (OZPN) and etioporphyrin I (EtpI). The results demonstrate that the crystal growth units may diverge from both the dominant solute species and the crystal structural units and inform that the correlation between the symmetry of a solute oligomer and the crystal structure is far from a general law.

OZPN: growth by incorporation of dimers that capture a minor fraction of the solute

Olanzapine (OZPN, 2-methyl-4-(4-methyl-1- piperazinyl)-10H-thieno-[2,3-b] [1,5] benzodiazepine, Fig. 1a) is a benzodiazepine derivative used to treat the positive (hallucinations and delusions) and negative (social withdrawal) symptoms of schizophrenia, bipolar disorder, and other psychoses,[44] which precipitates in more than 60 individual crystal forms.[45] In most of these forms OZPN molecules arrange in a centrosymmetric dimer, comprised of two conformational enantiomers (Fig. 1c).[45] The dominance of dimeric structures has encouraged the supposition that the dimers form in the solution, where they are expected to be the dominant species, and then incorporate in the crystal as a whole.[46, 47]

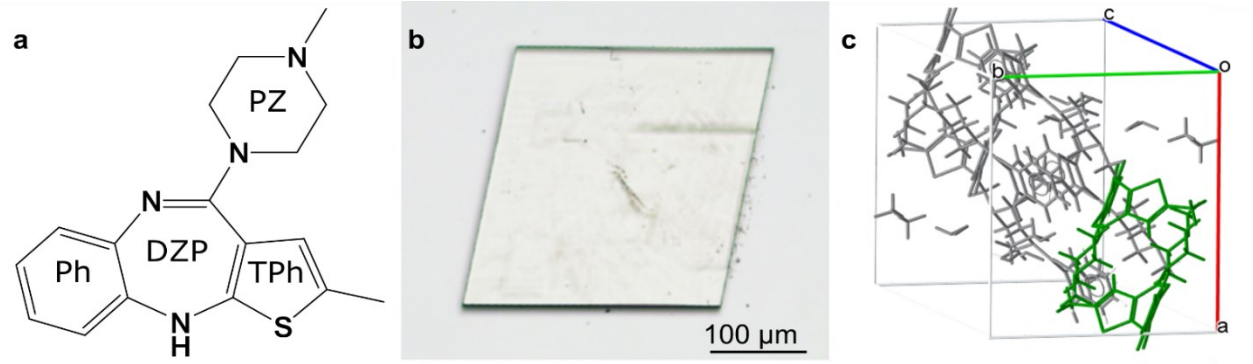

Fig. 1. The structure of OZPN and its crystals. a. The structure of the OZPN molecule: Ph, benzene; DZP, diazepine; TPh, thiophene; and PZ, piperazine rings. **b.** Optical micrograph of an OZPN crystal, in which the (002) face faces upwards. **c.** The crystal structure of the dihydrate ethanoate mixed solvate 2OZPN·EtOH·2H2O in space group $P2_1/c$ (Cambridge Structural Database REFCODE WEXQEW [48]). One centrosymmetric OZPN dimer is highlighted in green.

To test the third part of the "dimer is the growth unit" hypothesis for OZPN, that OZPN crystals grow by incorporation of dimers, we monitor the growth of 2OZPN·EtOH·2H_2O crystals from a 1/1 (v/v) ethanol/water mixture using time-resolved *in situ* AFM.[47] Crystals prepared by cooling crystallization are light yellow in color and show a rhombohedral morphology with large {002} faces parallel to the substrate (Fig. 1b) suitable for observation by atomic force microscopy (AFM); for details of the experiment procedures, see Ref. [49]. Time-resolved *in situ* AFM monitoring reveals that the {002} faces grow by incorporation of solute into steps produced by screw dislocations (Fig. 2b). [47] The step velocity v was determined from the slope of step displacement against a reference point as a function of time as OZPN steps grew at steady rates over extended periods. Assuming that steps grow by incorporation of solute monomers[50] suggests monomolecular reaction and generates a linear correlation between v and the solute concentration C_{OZPN}, $v = \beta\Omega(C_{OZPN} - C_e)$, where subtracting the solubility C_e accounts for the reversibility of molecular attachment. Here Ω is the molecular volume in the crystal, and β is an effective kinetic coefficient, which includes the kinetic parameters for the selected growth mechanism, direct incorporation or *via* adsorption on the terraces.[51, 52] Linear $v(C_{OZPN})$ correlations have been observed for numerous solution grown crystals.[10, 27, 29, 53-66] Surprisingly, OZPN displays a superlinear $v(C_{OZPN})$ dependence, which extends to concentrations more than twice the solubility C_e (Fig. 2c, d).

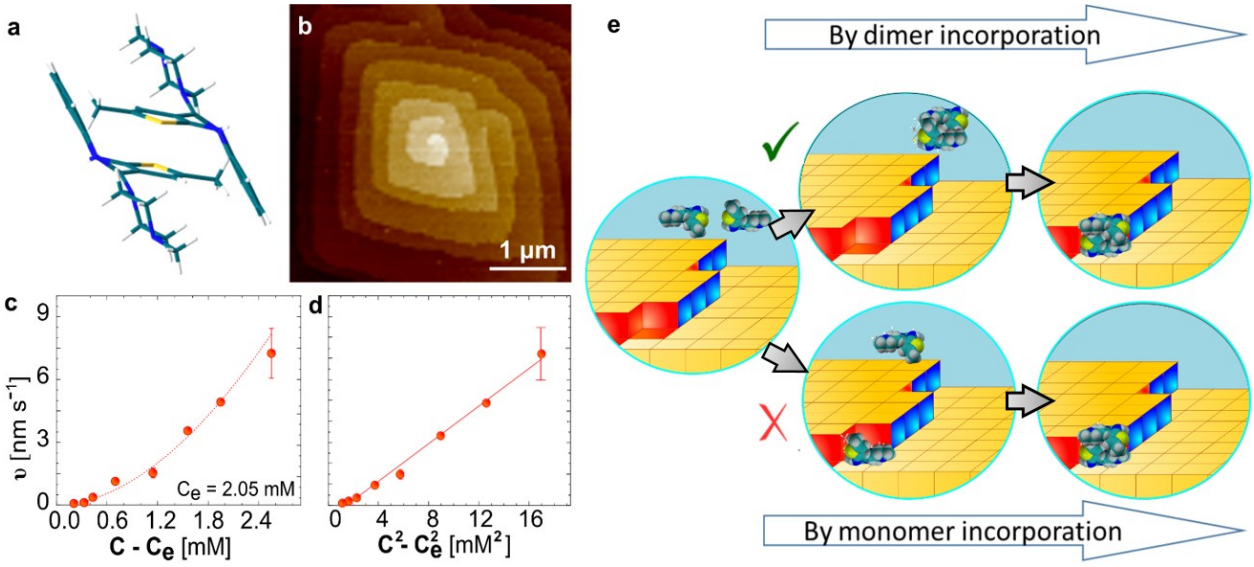

Fig. 2. The growth of OZPN crystals. a. The structure of the OZPN crystal dimer. **b.** *In situ* AFM image of the surface of a (002) face of an OZPN crystal at C = 3.87 mM. New crystal layers are generated by a screw dislocation. **c.** The velocity v of steps in the [110] direction as a function of OZPN concentration C in 1/1 (v/v) EtOH/H_2O. **d.** The linear correlation between v and $(C^2 - C_e^2)$ has R = 0.95. Dotted lines in **c** and **d** depict the relation $v = \beta_D K_D \Omega_D (C^2 - C_e^2)$, where β_D is the kinetic coefficient for growth by dimer incorporation, $\Omega_D = 2\Omega_M = 0.94$ nm^3 is the volume occupied by a dimer in the crystal, and K_D is the dimerization equilibrium constant. Error bars in **c** and **d** indicate the standard deviation of v determined as the slope of the displacement-time correlations. Data in c and d are from ref. [49]. **e.** Schematic of two alternative growth mechanisms. Upper path: two OZPN monomers form a dimer in the solution, which incorporates into the crystal as a whole. Lower path: the two monomers incorporate sequentially, forming a dimer in the crystal.

We excluded four potential causes of the apparent growth acceleration at high supersaturation:[49] mesoscopic OZPN-rich clusters,[47, 67] an additional source of OZPN molecules to the steps; inaccurate solubility; increasing kink density at higher supersaturation;[29, 50, 68] and step pinning by impurities.[53] We propose that the superlinear $v(C_{OZPN})$ is a consequence of crystal growth by incorporation of dimers present in equilibrium with OZPN monomers in the growth solution (Fig.2e). Elevated OZPN concentrations shift the dimerization equilibrium towards dimers and nonlinearly enhance the dimer concentration. Kinetic analysis[49] demonstrates that if monomers dominate in the solution, but growth occurs by the attachment dimers, then the step velocity v correlates with the total solute concentration C_{OZPN} as $v = \beta_D \Omega_D K_D (C_{OZPN}^2 - C_e^2)$, where β_D is the kinetic coefficient for growth by dimer incorporation, Ω_D is the volume that a dimer

occupies in the crystal, and K_D is the dimerization equilibrium constant. By contrast, if the crystals grow by incorporation of the majority monomers, then we recover thee expected linear correlation $v = \beta_M \Omega_M (C_{OZPN} - C_e)$, where β_M is the kinetic coefficient for growth by monomer incorporation and Ω_M is the volume that a monomer occupies in the crystal. Importantly, a liner rate law also obtains if the crystal grows by incorporation of dimers in a solution dominated by dimers, $v = \beta_D \Omega_M (C_{OZPN} - C_e)$; notably, in the latter case v scales with the monomer volume Ω_M.

This analysis reveals that if the dominant solute species, whether it be monomer or dimer, is the one that incorporates in the kinks, the kinetics of layer growth will be linear. If the crystals grow by incorporation of solute dimers that exist in equilibrium with a majority of monomers a quadratic correlation between the step velocity and the analytical concentration of the solute ensues. The $v(C_{OZPN})$ data for OZPN are consistent with this latter functional relation (Fig. 2c, d).

The discrepancy between the linear kinetic law expected for growth by incorporation of dimers, which capture a majority of the solute, and the superlinear $v(C_{OZPN})$ dependence measured by AFM is a first indication that dimers do not dominate in OZPN solutions. To further explore the monomer-dimer solute dynamics, we employ Raman spectroscopy; for details of the experiment procedures, see Ref. [49].. We compare OZPN spectra at a low concentration, 0.005 M, to spectra at relatively high concentrations, up to 0.043 M, and to spectra of the corresponding solid form, 2OZPN·EtOH·2H_2O, in which OZPN is arranged as dimers (Fig. 3a). To assign the origins of the observed peaks, we model spectra for an OZPN monomer and an OZPN dimer using density functional theory (DFT)[49] (Fig. 3a). The model spectra for the OZPN monomer show multiple Raman peaks between 1200 and 1500 cm^{-1} (Fig. 3a), whereas the model spectra for the dimer show strong peaks around 1050 cm^{-1} and in the range 1500-1600 cm^{-1}.[49]

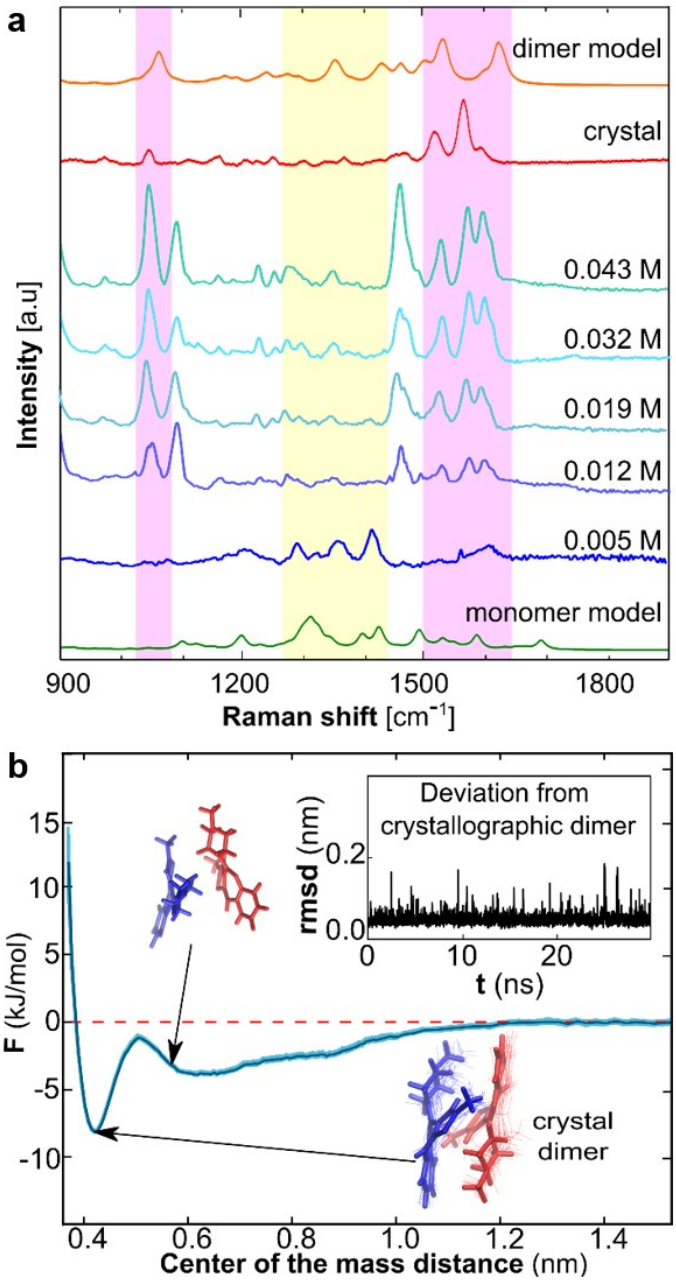

Fig. 3. OZPN dimers in solution. a. Raman spectra of OZPN dissolved in 1/1 (v/v) EtOH/H_2O at listed concentrations and of the solid crystalline solvate are compared to spectra for OZPN monomer and dimer calculated using DFT. Yellow stripe highlights characteristic monomer peaks, whereas pink stripes, those typical of dimers. **b.** The potential of mean force *F* between two OZPN monomers in 1/1 (v/v) EtOH/H_2O computed using all-atom umbrella sampling molecular dynamics. The line width represents the computational uncertainty. Insets: Top left, a representative configuration of the two monomers at separations longer than the deep minima. Top right, The root-mean-squared deviations of the positions of all OZPN atoms in the dimers occupying the deep minima from the dimer structure in the 2OZPN·EtOH·2H2O crystals as functions of time are small, indicating that the dimers assembled in the solution are nearly identical to the dimer found in the crystal structure. Lower right, representative snapshots of the

configuration of the dimer (the constituent monomers are shown in red and blue, respectively) occupying the deepest *F* minimum which is nearly identical to the dimer found in the crystal structure (one of the ten conformations is highlighted for clarity). Some of the spectra in a and the mean force potential in b are from ref. [49].

Raman spectra of OZPN water ethanoate solvate crystals show noticeable dimer peaks similar to spectra obtained for solution samples at high concentrations (Fig. 3a). The low-concentration solution spectra reveal strong monomer peaks and no of dimer peaks. Raman spectra at increasing intermediate concentrations in both solvents show gradual contraction of the monomer peaks and a growth in intensity of the dimer peaks (Fig. 3a). The concentration dependences of the monomer and dimer Raman peak intensities provides the opportunity to assess the OZPN dimerization constant K_D.[49] We obtain $K_D = 2.7 \pm 0.1$ M^{-1}. Mass balance calculations inform that the dimer concentration C_D in the growth solution is 0.01 mM at the solubility 2.05 mM; C_D increases to 0.05 mM at the highest tested total OZPN concentration in the growth studies, C = 4.45 mM (Fig. 2c). The superlinear increase of C_D dictates the quadratic $v(C)$ correlation measured by AFM (Fig. 2c, d).

All-atom umbrella sampling molecular dynamics (for details, see ref. [49]) assessment of the potentials of mean force *F* between two OZPN monomers in EtOH/H_2O reveal a sharp minimum at center-of-mass separations of 0.43 nm (Fig. 3b). The conformations of the two monomers occupying the minimum oscillate around the structure of the dimer present in most OZPN crystal forms (Fig. 3b, inset). At larger separations, the dimer dissociates, however, *F* exhibits a shallow secondary minimum that links to loose dimers with variable conformations (Fig. 3b). We evaluated the free energy of OZPN dimerization in EtOH/H_2O from the potential value at the deep minimum and obtained –8.1 kJ mol^{-1}.[49]The dimerization constant K_D was evaluated as the ratio of integrals of *F* over the closest range minimum, i.e., the bound state, and the unbound state and is 2.6±0.8 M^{-1}. The similarity of the computed K_Ds to the values determined from the concentration responses of the monomer and dimer Raman peaks presents an independent validation of the simulations. Further MD calculations identify the reason for faster growth by

dimers as their stronger adsorption on the crystal surface supplemented by additional dimerization on the surface, which creates a readily available pool of dimers that can incorporate as a whole into the steps .[49]

The results with OZPN establish a deviation from the classical mechanisms of crystallization, which assume that crystals grow by successive association of solute molecules as monomers. We show that a preformed centrosymmetric solute dimer is the preferred growth unit for OZPN crystals despite the fact dimers comprise a minority of the solute population in the solution bulk. Importantly, this study highlights that the growth unit can be identified by correlating solute oligomerization to the solute incorporation rate law. Furthermore, the kinetic, structural, and spectroscopic analyses of OZPN solutions and the growth of OZPN crystals emphasize the disparity between the majority species in the bulk solution, the microenvironment adjacent to the growth surface and both the crystal structure and the structure of the incorporating solute unit.

EtpI: distinct growth mechanisms of the anisotropic crystal faces

Etioporphyrin I (EtpI, Fig. 4a) represents a class of compounds whose solid-state structure (Fig. 4b) offers promising optical and electronic properties for use as semiconductors, solar cells, and field-effect transistors.[69-71] In contrast to OZPN, EtpI has a unique unsolvated triclinic crystal structure built of single molecules stacked in parallel pillars (Fig. 4c).[69] Currently the Cambridge Structural Database (CSD) search of etioporphyrin I results in single solid-state form belonging to the non-centrosymmetric P1 crystallographic symmetry group (Fig. 4c).

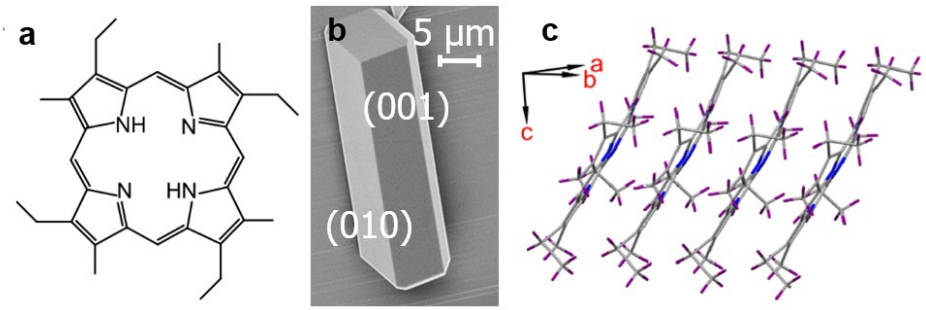

Fig. 4. EtpI and its crystals. a, The EtpI molecule. **b**, Scanning electron micrograph of an EtpI crystal. The (010) and (001) faces are labeled. **c**, Molecular arrangement of EtpI in the crystal; Cambridge Structural Database REFCODE WOBVUF.[69] Carbon is shown in grey, nitrogen in blue, and hydrogen in purple.

Owing to their nearly square cross-section, EtpI crystals expose two faces to AFM observation: (010) and (001). The presence of a (101) face in the crystal morphology enforces distinct shapes, parallelogram for the (010) face and trapeze for the (001) face. *In situ* AFM monitoring expose that similar to the (002) OZPN face, both {010} and {001} EtpI faces readily grow in 1-octanol by association of molecules into steps generated by screw dislocations (Fig. 5 a, b). Time resolved AFM measurements of the step velocity v reveal that on the (010) face, v scales linearly with the solute concentration C_{EtpI}, whereas on the (001) face v shows superlinear dependence of the step velocity v andC_{EtpI} (Fig. 5c, d).

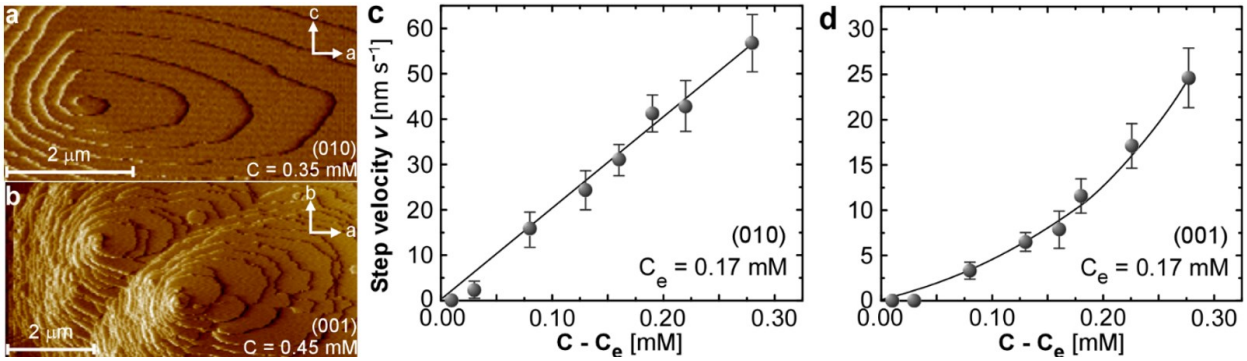

Fig. 5. The growth of (010) and (001) faces of EtpI crystals. a, **b**, Generation of new crystal layers by a screw dislocation outcropping on the respective face. **c, d**, The velocity v of steps in the [100] direction as a function of EtpI concentration C in octanol. Error bars denote standard deviation from the average of about 30 measurements for each data point. Solid lines correspond to best fits to linear, in C, and quadratic, in D, kinetics laws.

Eliminating the trivial reasons that may drive a superlinear $v(C)$ dependence (inaccurate solubility value, paucity of kinks, and step inhibition by uncontrolled foreign substances) the two distinct correlations manifest monomolecular kinetics of solute incorporation on the (010) face and bimolecular reaction on the (001) face. A feasible mechanism that guides the divergent kinetics laws on the two crystal faces relies on monomers that dominate the solute speciation. Step growth on the (010) face, which exhibits monomolecular incorporation rate law, selects the

monomers as incorporating species since this incorporation mode motivates faster step growth than incorporation of potential oligomers. By contrast, the bimolecular kinetics of step growth on the (010) face manifests two monomers combining into dimers, which remain a minority solute species, but still propel growth by dimers on the (010) face faster than by incorporation of the majority solute monomers.

We characterized the EtpI oligomerization in octanol solutions by vibrational spectroscopy—the concentration of EtpI in octanol, controlled by the low solubility C_e = 0.17 mM, is below the sensitivity of Raman detection on the background of strong octanol spectra—and augmented the spectroscopy by all-atom MD simulations of the dimerization equilibrium of EtpI dissolved in octanol. Similarly to OZPN, the two methods concertedly expose that the monomers represent the majority of the total C_{EtpI} and the monomer concentration increases proportionally to C_{EtpI}. This proportionality supports the proposal that the (010) face, on which the step velocity increases linearly with C_{EtpI}, grows by incorporation of monomers.

The concentration of dimers in a solution with total EtpI concentration equal to the solubility, 0.17 mM, is ca. 0.0002 mM and it increases to about 0.002 mM at the highest C_{EtpI} = 0.45 mM, at which step velocities were measured (Fig. 5).[72] The lower dimer content in EtpI solutions than in OZPN solutions is due to the lower total EtpI concentration, dictated by the lower solubility of this compound. The superlinear increase of the dimer concentration with higher C_{EtpI} manifests as quadratic increase of the step velocity on the (001) face, concurrently with the proposed mechanism of growth by dimer incorporation on that face. Notably, the good correspondence of the $v(C_{EtpI})$ correlation to a quadratic rate law minimizes the potential contributions of trimers and higher oligomers—expected to enforce an even steeper $v(C_{EtpI})$ increase—to growth on the (001) EtpI face.

The solute pathway into kinks and the selection of growth units

A solute molecule may arrive at a kink either directly from the solution[51, 73, 74] (Fig. 6a) or after adsorption on the terraces between steps, followed by diffusion towards the kinks[50, 52] (Fig. 6b). For olanzapine, detailed measurements of the velocities of closely spaced steps revealed that they grow substantially slower than steps separated by more than ca. 250 nm.[49] Furthermore, the dynamics of steps with uneven front and rear terraces indicated that solute incorporates into steps asymmetrically and the lower terrace is preferred as a solute conduit.[49] Both observations are incompatible with direct solute incorporation.[59, 60] Importantly, they comply with predictions of the surface diffusion models[32, 75-80] and argue that the solute species that incorporate into kinks on OZPN (002) crystal surfaces reach the steps after diffusion along the crystal surface, similarly to numerous solution grown crystals.[49, 59, 77, 79] All-atom MD simulations of adsorption of OZPN monomers and dimers established that faster step growth by dimers is due to their stronger adsorption on the terraces between steps and supplementary dimerization of monomers occurring in the adsorbed state.[49] This latter result may be interpreted to imply that the crystal surface is crucial for the selection of growth by dimer incorporation as it serves as a reservoir where dimers accumulate.

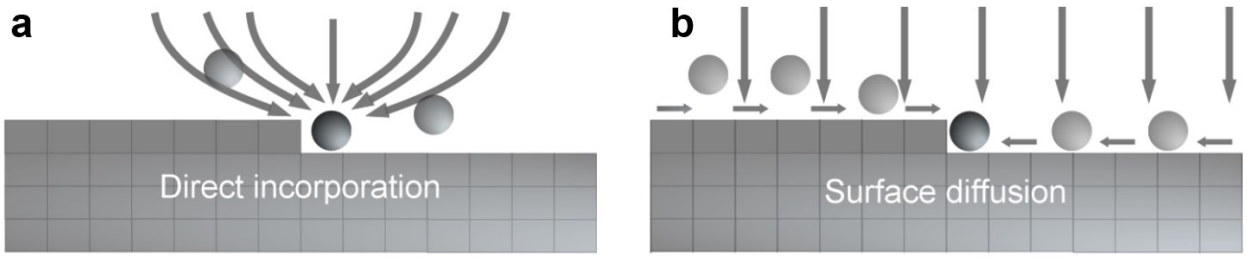

Fig. 6. Schematic of two pathways from solution to kinks: direct incorporation, in **a**, and *via* adsorption on the terraces followed by diffusion towards the steps in **b**. Arrows indicate supply fluxes of solute, depicted as spheres, towards the steps.

Mechanically transferring the OZPN insights to the two faces of EtpI would suggest that solute reaches the steps on the (001) face, which grows by associating dimers, via surface diffusion, whereas steps on the (010) face, which preferentially incorporate monomers, recruit

solute directly from the solution, where the monomers dominate. AFM measurements of the growth of steps of two distinct heights h, however, refute this conjecture. We compare the growth of steps as high as two lattice parameters to the growth of single-height steps. If solute reaches the steps via the crystal surface, the step supply field is constrained to two dimensions, which stunts the growth of steps of double height. Concurrently, analytical models of step growth mediated by surface diffusion predict that v scales with h^{-1}.[52, 77, 81]. By contrast, if the steps feed directly from the solution, the supply field is three-dimensional and abundant for twinned steps. Closed-form expressions for this growth mode predict negligible $v(h)$ correlation [51, 73]. Time resolved *in situ* AFM measurements reveal that on both the {001} and {010} faces the velocities of steps as high as the lattice parameter are close to those of steps of single height (Figs. 7, 8). The comparable rates of growth of twinned and single-height steps affirm that both faces of etioporphyrin I, uniquely, prefer the direct incorporation pathway.

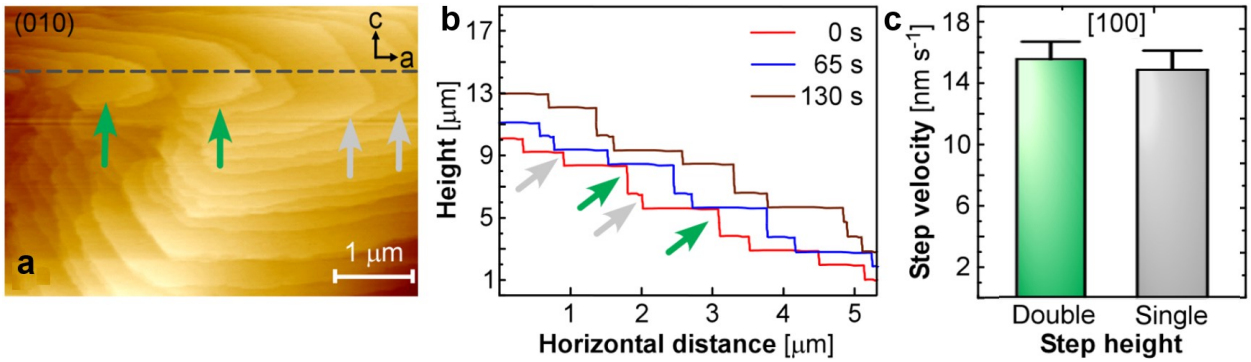

Fig. 7. Growth of single and double height steps on a (010) face of an EtpI crystal at C = 0.25 mM.. **a.** An AFM image of the growth of single (silver arrows) and double (green arrows) height steps of a (010) face **b.** The evolution of the surface profile along the dotted line in a. Double-height steps (green arrows) advance over lengths similar to those of single-height steps (silver arrows). **c.** Comparison of the velocities of single and double height steps. The averages of 10 double and 10 single height steps are shown. Error bars represent the respective standard deviations.

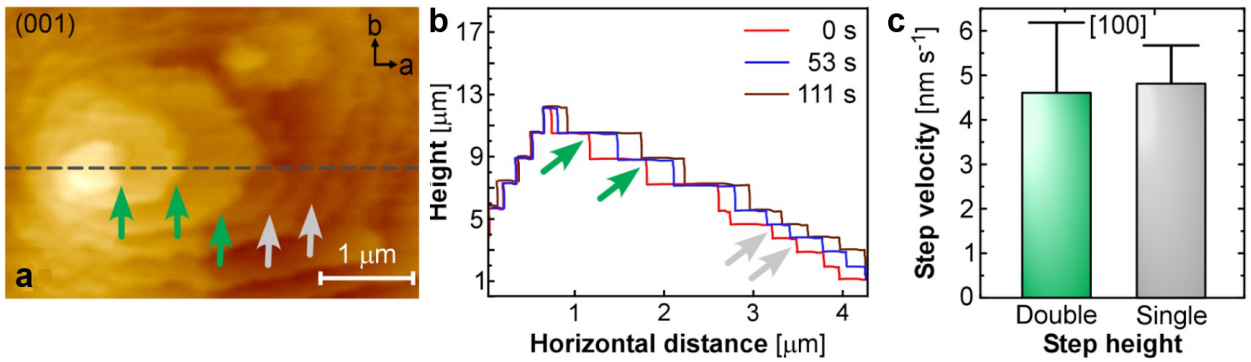

Fig. 8. Growth of single and double height steps on a (001) face of an EtpI crystal at *C* = 0.25 mM.. **a.** An AFM image of the growth of single (silver arrows) and double (green arrows) height steps of a (010) face **b.** The evolution of the surface profile along the dotted line in a. **c.** Comparison of the average velocities of single and double height steps. Error bars represent the standard deviations from the averages over measurements of 10 double and 10 single height steps.

Short of full scale MD simulations of incorporation of monomers and dimers into kinks on (001) and (010) faces of EtpI, we speculate that the selection of distinct solute species to incorporate into the kinks on the (010) and (001) faces of EtpI crystals is driven by the divergent structures of these two faces. The (010) face is relatively smooth (Fig. 9a) and the simple structure of the kink grants easy access for incorporation of the majority monomers. By contrast, the (001) face is pierced by dimples and grooves. We surmise that monomers may be trapped into the dimples at the step edge and erect growth-incompetent configurations, whereas dimers, which fit seamlessly into the dimples, provide for continuous growth.

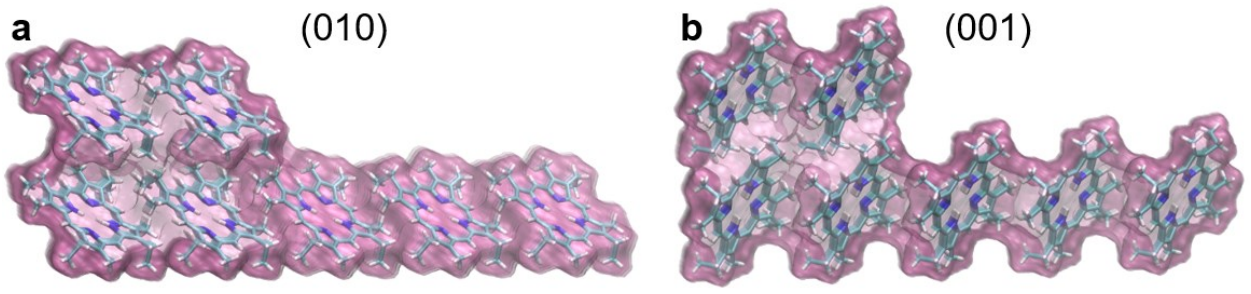

Fig. 9. Models of the molecular structures of steps on the (010), in **a**, and (001), in **b**, faces of EtpI crystals.

Importantly for the correlations between crystal symmetry and the growth unit, discussed here, the finding that the (001) EtpI face of grows by association of dimers, which reach the kinks

directly from the solution, announces that solute adsorption on crystal surfaces that prefer dimers and promote further dimerization, as with OZPN, is not a necessary condition for this growth mode.

Conclusions

Olanzapine and etioporphyrin I reveal the lack of general rules to correlate the majority solute species and crystal structural blocks that carry the crystal symmetry. Olanzapine is an example where the crystal growth unit diverges from the majority solute monomers and matches a centrosymmetric crystal structural element. With etioporphyrin I, the monomeric crystal growth unit selected by one of the faces is identical to both the crystal structural element and the majority solute species, whereas the dimeric growth unit on the other face represents just one of the elements of a vast variety of dimers that cohabit in the solution and diverge from the crystal lattice motif.

Crystal symmetry, unfortunately, does not open a shortcut to identifying the crystal growth unit and cannot reliably simplify theories and models that target molecular-level understanding of crystal growth.

Acknowledgments

This work was supported by the National Science Foundation (award no. DMR-2128121), the Welch Foundation (Grant E-1882), and the State of Texas through the Texas Center for Superconductivity at the University of Houston. Computational resources were provided by the Hewlett Packard Enterprise Data Science Institute at the University of Houston and the Texas Advanced Computing Center at the University of Texas at Austin. The authors acknowledge the CMAC National Facility, housed within the University of Strathclyde's Technology and Innovation Centre, and funded with a UKRPIF (UK Research Partnership Investment Fund) capital award, SFC ref H13054, from the Higher Education Funding Council for England (HEFCE) and the

EPSRC Future Continuous Manufacturing and Advanced Crystallisation Research Hub (Grant Ref: EP/P006965/1).

Authors' contributions

[‡]These authors contributed equally to this work

[*]Send correspondence to vekiov@uh.edu

References

1. B. K. Vainshtein, *Fundamentals of Crystals: Fundamentals of Crystals. Symmetry, and Methods of Structural Crystallography*, Springer, Berlin, Second edn., 1994.
2. C. Kittel, *Introduction to solid state physics*, John Wiley and Sons, New York, 6 edn., 1986.
3. N. N. Greenwood and A. Earnshaw, *Chemistry of the Elements. 2nd Edition*, Butterworth-Heinemann, 1997.
4. V. M. A. Rajendran, *Materials science*, Tata McGraw-Hill Pub., New Delhi, 2004.
5. Y. Saigusa, in *Advanced Piezoelectric Materials (Second Edition)*, ed. K. Uchino, Woodhead Publishing, 2017, DOI: https://doi.org/10.1016/B978-0-08-102135-4.00005-9, pp. 197-233.
6. V. F. Petrenko and R. W. Whitworth, *Physics of Ice*, Oxford University Press, Oxford, 2002.
7. T. V. Barker, *Nature*, 1923, **111**, 632.
8. A. Gavezzotti, *Accounts Chem. Res.*, 1994, **27**, 309-314.
9. J. Bernstein, *Polymorphism in Molecular Crystals*, Oxford University Press, Oxford, 2007.
10. O. Gliko, N. Neumaier, W. Pan, I. Haase, M. Fischer, A. Bacher, S. Weinkauf and P. G. Vekilov, *J. Amer. Chem. Soc.*, 2005, **127**, 3433-3438.
11. D. Li, M. H. Nielsen, J. R. I. Lee, C. Frandsen, J. F. Banfield and J. J. De Yoreo, *Science*, 2012, **336**, 1014-1018.
12. J. Baumgartner, A. Dey, P. H. H. Bomans, C. Le Coadou, P. Fratzl, N. A. J. M. Sommerdijk and D. Faivre, *Nature Materials*, 2013, **12**, 310.
13. H. Coelfen and M. Antionetti, *Journal*.
14. J. J. De Yoreo, P. U. P. A. Gilbert, N. A. J. M. Sommerdijk, R. L. Penn, S. Whitelam, D. Joester, H. Zhang, J. D. Rimer, A. Navrotsky, J. F. Banfield, A. F. Wallace, F. M. Michel, F. C. Meldrum, H. Cölfen and P. M. Dove, *Science*, 2015, **349**, aaa6760.
15. S. Lee, H. S. Wi, W. Jo, Y. C. Cho, H. H. Lee, S.-Y. Jeong, Y.-I. Kim and G. W. Lee, *Proceedings of the National Academy of Sciences*, 2016, **113**, 13618-13623.
16. Y. Politi, R. A. Metzler, M. Abrecht, B. Gilbert, F. H. Wilt, I. Sagi, L. Addadi, S. Weiner and P. U. P. A. Gilbert, *Proceedings of the National Academy of Sciences*, 2008, **105**, 17362-17366.
17. A. I. Lupulescu and J. D. Rimer, *Science*, 2014, **344**, 729-732.
18. M. J. Thomason, C. R. Seabourne, B. M. Sattelle, G. A. Hembury, J. S. Stevens, A. J. Scott, E. F. Aziz and S. L. M. Schroeder, *Faraday Discussions*, 2015, **179**, 269-289.
19. W. Tang, H. Mo, M. Zhang, S. Parkin, J. Gong, J. Wang and T. Li, *The Journal of Physical Chemistry B*, 2017, **121**, 10118-10124.

20. V. Cheynier, R. Schneider, J.-M. Salmon and H. Fulcrand, in *Comprehensive Natural Products II*, eds. H.-W. Liu and L. Mander, Elsevier, Oxford, 2010, DOI: https://doi.org/10.1016/B978-008045382-8.00088-5, pp. 1119-1172.
21. A. Idrissi, P. Damay, K. Yukichi and P. Jedlovszky, *The Journal of Chemical Physics*, 2008, **129**, 164512.
22. C. A. Hunter, J. F. McCabe and A. Spitaleri, *CrystEngComm*, 2012, **14**, 7115-7117.
23. K. R. Back, R. J. Davey, T. Grecu, C. A. Hunter and L. S. Taylor, *Crystal Growth & Design*, 2012, **12**, 6110-6117.
24. R. Davey, G. Dent, R. Mughal and S. Parveen, *Crystal Growth & Design*, 2006, **8**, 1788-1796.
25. S. Parveen, R. J. Davey, G. Dent and R. G. Pritchard, *Chemical Communications*, 2005, DOI: 10.1039/B418603F, 1531-1533.
26. M. Gardner, A. J. Guerin, C. A. Hunter, U. Michelsen and C. Rotger, *New Journal of Chemistry*, 1999, **23**, 309-316.
27. S.-T. Yau, D. N. Petsev, B. R. Thomas and P. G. Vekilov, *J. Mol. Biol.*, 2000, **303**, 667-678.
28. S.-T. Yau, B. R. Thomas, O. Galkin, O. Gliko and P. G. Vekilov, *Proteins: Structure, Function, Genetics*, 2001, **43**, 343-352.
29. S.-T. Yau, B. R. Thomas and P. G. Vekilov, *Phys. Rev. Lett.*, 2000, **85**, 353-356.
30. S.-T. Yau, B. R. Thomas and P. G. Vekilov, *J. Crystal Growth*, 2001, **232**, 188-194.
31. M. Sleutel, D. Maes, L. Wyns and R. Willaert, *Crystal Growth & Design*, 2008, **8**, 4409-4414.
32. M. Sleutel, C. Vanhee, C. V. de Weerdt, K. Decanniere, D. Maes and L. W. R. Willaert, *Crystal Growth & Design*, 2008, **8**, 1173-1180.
33. M. Sleutel, R. Willaert, C. Gillespie, C. Evrard, L. Wyns and D. Maes, *Crystal Growth & Design*, 2009, **9**, 497-504.
34. M. Sleutel, J. Lutsko, A. E. S. Van Driessche, M. A. Durán-Olivencia and D. Maes, *Nat Commun*, 2014, **5**.
35. A. J. Malkin, Y. G. Kuznetsov, R. W. Lucas and A. McPherson, *J. Struct. Biol.*, 1999, **127**, 35-43.
36. A. J. Malkin, Y. G. Kuznetsov and A. McPherson, *J. Crystal Growth*, 1999, **196**, 471-488.
37. Y. G. Kuznetsov, A. J. Malkin, R. W. Lucas, M. Plomp and A. McPherson, *J Gen Virol*, 2001, **82**, 2025-2034.
38. A. McPherson, A. J. Malkin, Y. G. Kuznetsov and M. Plomp, *Acta Crystallogr D Biol Crystallogr*, 2001, **57**, 1053-1060.
39. A. J. Malkin and A. McPherson, in *From fluid-solid interfaces to nanostructural engineering. vol. 2. Assembly in hybrid and biological systems.*, eds. J. J. De Yoreo and X. Y. Lui, Plenum/Kluwer Academic, New York, 2004, pp. 201-238.
40. A. J. Malkin and R. E. Thorne, *Methods*, 2004, **34**, 273-299.
41. D. K. Georgiou and P. G. Vekilov, *Proc. Natl. Acad. Sci. USA*, 2006, **103**, 1681-1686.
42. S.-T. Yau and P. G. Vekilov, *Nature*, 2000, **406**, 494-497.
43. S.-T. Yau and P. G. Vekilov, *J. Am. Chem. Soc.*, 2001, **123**, 1080-1089.
44. B. Fulton and K. L. Goa, *Drugs*, 1997, **53**, 281-298.
45. R. M. Bhardwaj, L. S. Price, S. L. Price, S. M. Reutzel-Edens, G. J. Miller, I. D. H. Oswald, B. F. Johnston and A. J. Florence, *Crystal Growth & Design*, 2013, **13**, 1602-1617.
46. Y. Sun, C. J. Tilbury, S. M. Reutzel-Edens, R. M. Bhardwaj, J. Li and M. F. Doherty, *Crystal Growth & Design*, 2018, **18**, 905-911.
47. M. Warzecha, R. Guo, R. M. Bhardwaj, S. M. Reutzel-Edens, S. L. Price, D. A. Lamprou and A. J. Florence, *Crystal Growth & Design*, 2017, **17**, 6382-6393.
48. I. Wawrzycka-Gorczyca, P. Borowski, J. Osypiuk-Tomasik, L. Mazur and A. Koziol, *Journal of Molecular Structure*, 2007, **830**, 188-197.

49. M. Warzecha, L. Verma, B. F. Johnston, J. C. Palmer, A. J. Florence and P. G. Vekilov, *Nature Chemistry*, 2020, **12**, 914-920.
50. W. K. Burton, Cabrera, N. &. Frank, F.C., *Phil. Trans. Roy. Soc. London Ser. A*, 1951, **243**, 299- 360.
51. A. A. Chernov, *Modern Crystallography III, Crystal Growth,*, Springer, Berlin, 1984.
52. G. H. Gilmer, R. Ghez and N. Cabrera, *J. Crystal Growth*, 1971, **8**, 79-93.
53. J. J. De Yoreo and P. G. Vekilov, in *Biomineralization*, 2003, vol. 54, pp. 57-93.
54. J. J. De Yoreo, T. A. Land and B. Dair, *Phys. Rev. Lett.*, 1994, **73**, 838-841.
55. T. A. Land, A. J. Malkin, Y. G. Kuznetsov, A. McPherson and J. J. Deyoreo, *Physical Review Letters*, 1995, **75**, 2774-2777.
56. H. H. Teng, P. M. Dove, C. A. Orme and J. J. De Yoreo, *Science*, 1998, **282**, 724-727.
57. T. A. Land, T. L. Martin, S. Potapenko, G. T. Palmore and J. J. De Yoreo, *Nature*, 1999, **399**, 442 - 445.
58. Y. G. Kuznetsov, A. A. Chernov, P. G. Vekilov and I. L. Smol'skii, *Sov. Phys.-Crystallogr.*, 1987, **32**, 584-587.
59. P. G. Vekilov, Y. G. Kuznetsov and A. A. Chernov, *J. Crystal Growth*, 1992, **121**, 643-655.
60. P. G. Vekilov, Y. G. Kuznetsov and A. A. Chernov., *J. Crystal Growth*, 1992, **121**, 44-52.
61. P. G. Vekilov, in *Studies and Concepts in Crystal Growth*, ed. H. Komatsu, Pergamon, Oxford, 1993, pp. 25-49.
62. P. G. Vekilov and F. Rosenberger, *J. Crystal Growth*, 1996, **158**, 540-551.
63. P. G. Vekilov and F. Rosenberger, *J. Crystal Growth*, 1998, **186**, 251-261.
64. O. Gliko, I. Reviakine and P. G. Vekilov, *Phys. Rev. Lett*, 2003, **90**, 225503.
65. D. N. Petsev, K. Chen, O. Gliko and P. G. Vekilov, *Proc. Natl. Acad. Sci. USA*, 2003, **100**, 792-796.
66. Y. Qutub, I. Reviakine, C. Maxwell, J. Navarro, E. M. Landau and P. G. Vekilov, *Journal of Molecular Biology*, 2004, **343**, 1243-1254.
67. M. Warzecha, M. S. Safari, A. J. Florence and P. G. Vekilov, *Crystal Growth & Design*, 2017, **17**, 6668-6676.
68. M. A. Lovette and M. F. Doherty, *Physical Review E*, 2012, **85**, 021604.
69. C.-M. Che, H.-F. Xiang, S. S.-Y. Chui, Z.-X. Xu, V. A. L. Roy, J. J. Yan, W.-F. Fu, P. T. Lai and I. D. Williams, *Chemistry – An Asian Journal*, 2008, **3**, 1092-1103.
70. M. H. Hoang, Y. Kim, M. Kim, K. H. Kim, T. W. Lee, D. N. Nguyen, S.-J. Kim, K. Lee, S. J. Lee and D. H. Choi, *Advanced Materials*, 2012, **24**, 5363-5367.
71. M. H. Hoang, Y. Kim, S.-J. Kim, D. H. Choi and S. J. Lee, *Chemistry – A European Journal*, 2011, **17**, 7772-7776.
72. L. Verma, M. Warzecha, R. Chakrabarti, V. G. Hadjiev, J. C. Palmer and P. G. Vekilov, *Israel Journal of Chemistry*.
73. A. A. Chernov, *Sov. Phys. Uspekhi*, 1961, **4**, 116-148.
74. A. A. Chernov, *Contemp. Phys.*, 1989, **30**, 251-276.
75. M. Maruyama, K. Tsukamoto, G. Sazaki, Y. Nishimura and P. G. Vekilov, *Crystal Growth & Design*, 2009, **9**, 127-135.
76. G. Sazaki, M. Okada, T. Matsui, T. Watanabe, H. Higuchi, K. Tsukamoto and K. Nakajima, *Crystal Growth & Design*, 2008, **8**, 2024-2031.
77. T. A. Land, J. J. DeYoreo and J. D. Lee, *Surf. Sci.*, 1997, **384**, 136-155.
78. K. N. Olafson, M. A. Ketchum, J. D. Rimer and P. G. Vekilov, *Crystal Growth & Design*, 2015, **15**, 5535-5542.
79. K. N. Olafson, J. D. Rimer and P. G. Vekilov, *Physical Review Letters*, 2017, **119**, 198101.
80. G. Ehrlich and F. G. Hudda, *J. Chem. Phys.*, 1966, **44**, 1039-1052.
81. K. N. Olafson, M. A. Ketchum, J. D. Rimer and P. G. Vekilov, *Proceedings of the National Academy of Sciences*, 2015, **112**, 4946-4951.

Table of Contents Graphic

Table of Contents Text

The structures of the dominant solute species and of the incorporating solute complexes do not correlate with the symmetry of the crystal lattice. Crystal symmetry provides no shortcuts on the road to understanding and control of crystallization.